Wigner Crystallization in inhomogeneous one dimensional wires

Erich J. Mueller
Laboratory of Atomic and Solid State Physics, Cornell University, Ithaca, New York 14853
(Dated: October 29, 2004)

We explore the theory of electrons confined by one dimensional power law potentials. We calculate the density profile in the high density electron gas, the low density Wigner crystal, and the intermediate regime. We extract the momentum space wavefunction of the electron at the Fermi surface, which can be measured in experiments on tunneling between parallel wires. The onset of localization leads to a dramatic broadening of the momentum space wavefunction together with pronounced sharpening (in energy) of the tunneling spectrum.

PACS numbers: 73.21.Hb, 71.10.Pm, 73.23.Hk, 71.10.Hf

Advances in microprocessing have enabled scientists to construct ultra-high mobility one dimensional wires with transverse size $d_\perp \approx 20$nm, which is sufficiently small to freeze out all transverse electronic motion[1] . By allowing tunneling between two such parallel wires, Auslaender et al.[2] have been able to map out the spectrum of elementary excitations, providing good evidence of spin-charge separation. Further experiments have found evidence of electronic localization in these wires when a gate electrode is used to deplete the density of electrons[3]. This localization is possibly caused by an interaction driven transition into a Wigner crystal state[4,5], where each electron is localized by repulsion from its neighbors. Here we investigate the theory of such crystallization in one dimensional wires.

The wires used in these experiments are not infinitely long. Their finite length, which is controlled by electrostatic potentials, leads to striking fringes in the tunneling spectrum[6]. These fringes cannot be explained by particles bounded by 'infinite walls', but require a more accurate modeling of the confinement. Tserkovnyak et al.[6] found that the experimental results were consistent with a power-law potential $V_{\rm ext}(x) = V_0 x^\beta$, with $6 < \beta < 7$. In discussing experimental signatures of crystallization in these systems, we must take into account this same physics, and explore the interplay between the external confining potential and the interparticle Coulomb repulsion. Due to the influence of the gate electrode, the electrons in the localization experiment[3] feel a complicated potential, with two minima separated by a barrier.

After presenting our model (sec. I) and reviewing how tunneling measurements are related to microscopic properties (sec. II) we introduce a series of mean field approximations: a Thomas-Fermi description of the high density electron gas (sec. III); a semiclassical description of the Wigner crystal (sec. IV); and a Hartree-Fock description of the cross-over (sec. V). These models provide direct insight into the experimental signatures of this transition. Our approach complements prior theoretical work, which predominantly treated homogeneous infinite systems[7], small numbers of electrons[8], or infinite square well potentials[9].

I. MODEL

We consider a gas of electrons with $\sigma = 2$ spin states confined to a one dimensional wire, experiencing an external potential $V_{\rm ext}(x)$, where x is the coordinate along the wire. The electrons interact through pairwise three dimensional coulomb interactions, $U_{3d}(r_i - r_j) = e^2/(4\pi\epsilon|r_i - r_j|) = (\hbar^2/m^* a)1/|r_i - r_j|$, where ϵ is the dielectric constant of the medium and m^* is the electrons effective mass. Using parameters for n-doped GaAs ($\epsilon \approx 13, m^* \approx 0.067 m_e$, where m_e is the free-space electron mass), the effective Bohr radius is quite large, $a \approx 10^{-8}$m. In this wire, the electronic wavefunction has a transverse size $d_\perp \approx 20$nm. Integrating out these transverse dimensions, the electrons feel a regularized Coulomb interaction $U(r) = (\hbar^2/m^* a) f_{d_\perp}(r_i - r_j)$. Two useful regularizations are $f_d^{(1)}(x) = (x^2 + d^2)^{-1/2}$ and $f_d^{(2)}(x) = {\rm Min}(|x|^{-1}, d^{-1})$, where Min(x, y) is the smaller of x and y. As $d_\perp \to 0$ the exact form of the regularization becomes unimportant. Here we mostly rely on $f^{(2)}$.

One estimates the importance of correlations caused by the Coulomb interactions by comparing the interaction energy between two neighboring particles $E_{\rm int} = \hbar^2 n/a m^*$ to the Fermi (kinetic) energy $\mathcal{E}_f = k_f^2/2m^* = 2\pi^2\hbar^2 n^2/\sigma m^*$, where n is the one dimensional density of particles, and we have assumed $n d_\perp \ll 1$. Kinetic energy dominates at high densities, when $na \gg 1/2\pi^2$. In that limit one expects to find a liquid state, where electrons are delocalized. Conversely, when $na \ll 1/2\pi^2$, the Coulomb interaction dominates, and a Wigner crystal should be formed.

As a compromise between experimental relevance and simplicity we concentrate on power law potentials $V_{\rm ext}(x) = (\hbar^2/2m^*) x^\beta w^{-\beta-2}$, where w, which parameterizes the potential strength, roughly coincides with the size of the single particle ground state in this potential. For the relatively flat (large β) potentials used in experiments, w also roughly coincides with the 'lithographic length,' $L_{\rm lith}$, which is the physical distance between the gates which generate the potential barriers. Analysis of experimental data by Tserkovnyak et al.[6] show that $w \approx 3\mu m$. Taking the density of electrons to be

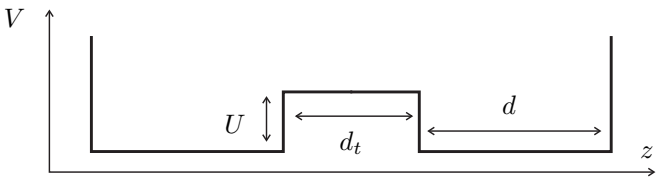

FIG. 1: Model of potential transverse to the two wires.

$n \approx N/w$, one expects crystallization when $N < N^*$, with $N^* \sim 20$.

II. TUNNELING BETWEEN PARALLEL WIRES

The experiments of Auslaender et al.[2] measure the tunneling current between the short wire described in section I, and a parallel long wire, which we will take to be infinite and uniform. Momentum is conserved in the tunneling. The wires are separated by $d_t \approx 6$nm, and the barrier separating the wires has height $U \approx 300$meV, arising from the conduction band offset between the GaAs wires, and the intervening AlGaAs. Using gate electrodes, the experimentalists control the chemical potential difference δV between the wires.[10] A magnetic field, perpendicular to the wires, gives a momentum kick $Q = eBd_t/\hbar$ to a tunneling electron[2]. We therefore consider the tunneling Hamiltonian,

$$\hat{H}_t = -T\sum_\sigma \int \frac{dk}{2\pi} e^{i(\delta V)t}\hat{\phi}^\dagger_\sigma(k+Q)\hat{\psi}_\sigma(k) + \text{H.C.}, \quad (1)$$

where $\hat{\psi}_\sigma(k) = \int dx\, e^{-ikx}\,\hat{\psi}_\sigma(x)$ and $\hat{\phi}_\sigma(k) = \int dx\, e^{-ikx}\,\hat{\phi}_\sigma(x)$ are respectively the operators which annihilate particles with momentum k and spin σ in the short and long wire. The magnitude of the tunneling matrix element T is estimated by examining the energy states in the double square well geometry sketched in figure 1. This one-dimensional potential is a crude model of the physics transverse to the wires. We can identify $t \approx \delta E/2$, where δE is the energy splitting between the two lowest energy single particle states. In the limit of a deep, wide barrier ($U \gg (\hbar^2/m^* d_t^2), (\hbar^2/m^* d_\perp^2)$), one finds

$$\delta E/2 = \frac{2\pi^2\hbar^2}{m^* d_\perp^3 \kappa} e^{-\kappa d_t}, \quad (2)$$

where $\hbar^2\kappa^2/2m^* = U$ (so numerically $\kappa \approx 0.2$/nm). which gives $T \approx 30$meV, which should be compared to the spacing of states transverse to the wire, $\delta E = 4\pi^2\hbar^2/m^*_{\text{eff}} d_\perp^2 \approx 1$eV. Due to this separation of scales, we treat H_t perturbatively.

A. Formal expression for tunneling current

The current operator, defined by $I(t) = -\partial N_\psi/\partial_t$, where $\hat{N}_\psi = \int \frac{dk}{2\pi}\sum_\sigma \hat{\psi}^\dagger_\sigma(k)\hat{\psi}_\sigma(k)$ is the number of particles in the short wire, is given by

$$\hat{I}(t) = -T\int \frac{dk}{2\pi}\sum_\sigma \text{Im}\left[e^{i\delta V t}\hat{\phi}^\dagger_\sigma(k+Q,t)\hat{\psi}_\sigma(k,t)\right]. \quad (3)$$

To lowest order in T, the tunneling current is

$$\langle I(t)\rangle = \int d\tau \frac{1}{i}\theta(t-\tau)\langle[I(t), H_t(\tau)]\rangle \quad (4)$$

$$= T^2 A_I(Q, \omega = \delta V), \quad (5)$$

where the spectral density of current fluctuations is related to the retarded current response function by $A_I(q,\omega) \equiv 2\text{Im}\chi^R_I(q,\omega)$, where $\chi^R_I(q,\omega) = \int dt\, e^{i\omega t}\,(\theta(t)/i)\,[\chi^>_I(q,t) - \chi^<_I(q,t)]$, with $\chi^>_I(q,t) = \int \frac{dk}{2\pi}\frac{dk'}{2\pi}\sum_\sigma \langle\hat{\phi}^\dagger_\sigma(k+q,t)\hat{\psi}_\sigma(k,t)\hat{\psi}^\dagger_\sigma(k',0)\hat{\phi}_\sigma(k'+q,0)\rangle$ and $\chi^<_I(q,t) = \int \frac{dk}{2\pi}\frac{k'}{2\pi}\sum_\sigma \langle\hat{\psi}^\dagger_\sigma(k',0)\hat{\phi}_\sigma(k'+q,0)\hat{\phi}^\dagger_\sigma(k+q,t)\hat{\psi}_\sigma(k,t)\rangle$. Assuming that in the absence of tunneling the electrons in the two wires are independent,[11] the expectation values can be factored, leading to

$$A_I(q,\omega) = \int \frac{dk}{2\pi}\frac{dk'}{2\pi}\sum_\sigma \int \frac{d\nu}{2\pi}\left[G^<_{\phi\sigma}(k,k';\nu)G^>_{\psi\sigma}(k+q,k'+q;\nu-\omega) - G^>_{\phi\sigma}(k,k';\nu)G^<_{\psi\sigma}(k+q,k'+q;\nu-\omega)\right] \quad (6)$$

$$= \int \frac{dk}{2\pi}\frac{dk'}{2\pi}\sum_\sigma \int \frac{d\nu}{2\pi}\left[f(\nu) - f(\nu-\omega)\right] A_{\psi\sigma}(k,k';\nu)A_{\phi\sigma}(k+q,k'+q;\nu-\omega), \quad (7)$$

where the single particle Greens functions $G^{>/<}_{\phi\,\sigma}(k,k';\omega) = \int dt\, e^{i\omega t}G^{>/<}_{\phi\,\sigma}(k,k';t)$, are given by $G^>_{\phi\,\sigma}(k,k';t) = \langle\phi_\sigma(k,t)\phi^\dagger_\sigma(k',0)\rangle, G^<_{\phi\,\sigma}(k,k';t) = -\langle\phi^\dagger_\sigma(k',0)\phi_\sigma(k,t)\rangle$, and equivalent expressions hold for $G^{>/<}_{\psi\,\sigma}(k,k',\omega)$. These Greens functions are related to the appropriate single particle spectral density by $G^>(\omega) = [1-f(\omega)]A(\omega)$ and $G^<(\omega) = f(\omega)A(\omega)$, where $f(\omega) = [e^{\beta(\omega-\mu)}+1]^{-1}$ is the Fermi function.

If we use the free electron spectral density for the long wire, $A_{\phi\,\sigma}(k,k';\omega) = (2\pi)^2\delta(k-k')\delta(\omega - k^2/2m^*)$, one arrives at the simple result that the tunneling current is

a direct measure of the single particle spectral density in the short wire,

$$\begin{aligned} A_I(\omega,q) &= \int \frac{dk}{2\pi}\sum_\sigma \left[f(\omega+k^2/2m^*)-f(k^2/2m^*)\right] \\ &\quad \times A_{\psi\,\sigma}(k-q,\omega+k^2/2m^*) \qquad (8)\\ &\approx \beta\omega\int\frac{dk}{2\pi}\sum_\sigma f_k(1-f_k)A_{\psi\,\sigma}(k-q,k^2/2m^*), \end{aligned}$$

where the last line neglects terms of order ω^2, and uses $f_k = f(k^2/2m^*)$.

At zero temperature, the Fermi functions become step functions and to lowest order in ω, equation (8) becomes

$$A_I(\omega,q) = \frac{\omega}{2\pi}\sqrt{\frac{m^*}{2\mathcal{E}_f}}\sum_\sigma\Big[A_{\psi\,\sigma}(\sqrt{2m^*\mathcal{E}_f}-q,\mathcal{E}_f) + A_{\psi\,\sigma}(-\sqrt{2m^*\mathcal{E}_f}-q,\mathcal{E}_f)\Big]. \qquad (9)$$

B. General Features

From the definition $A_{\psi\,\sigma}(k,\omega) = G^{>}_{\psi\,\sigma}(k,\omega) + G^{<}_{\psi,\sigma}(k,\omega)$, the single particle spectral density can be written as

$$A_{\psi\,\sigma}(k,\omega) = \frac{2\pi}{Z}\sum_{if} e^{-\beta(E_i-\mu N_i)}\left[\left|\langle i|\hat\psi_\sigma(k)|f\rangle\right|^2\delta(\omega-(E_f-E_i)) - \left|\langle f|\hat\psi_\sigma(k)|i\rangle\right|^2\delta(\omega-(E_i-E_f))\right] \qquad (10)$$

where $|i\rangle$ represents a many body state containing N_i electrons and possessing energy E_i. Normalization is given by the grand partition function $Z = \sum_i e^{-\beta(E_i-\mu N_i)}$. At zero temperature, the sum over i is omitted, and $|i\rangle$ is replace by the ground state.

One thus sees that current flows whenever momentum and energy can be conserved in the tunneling process. The magnitude of the current is set by the degree of overlap between states with different particle number.

When the electrons become localized in a Wigner crystal, the overlap between states with different particle number becomes extremely small (because removing a particle results in rearrangement of the entire crystal – a form of orthogonality catastrophe). Consequently, the average tunneling current should drop. This drop in average current is accompanied by a sharpening of line-widths and does not lead to a complete loss of the experimental signal. Instead, it leads to "coulomb-blockade" type peaks, where current only flows for discrete values of δV.

One will see discrete peaks if the line width is small compared to the level spacing in the short wire, $\delta E \sim (2\pi)^2\hbar^2/m^*w^2 \sim 0.05$meV. Assuming that the lifetime is only due to coupling between the two wires, then the line width is given by an expression very similar to that for the tunneling current. Since T is large on the scale of δE, one will only see these discrete peaks once the overlaps in (10) become extremely small.

C. Independent particle approximation

In an independent particle picture (such as Hartree-Fock), $A_{\psi\,\sigma}(k,\omega) = \sum_j |\phi_{j\,\sigma}(k)|^2\, 2\pi\delta(\omega - E_{j\,\sigma})$, where $\phi_{j,\sigma}(k)$ is the momentum space wavefunction of the j's single electron orbital of spin σ particles, with energy $E_{j\,\sigma}$. In general $\phi_{j\uparrow} \neq \phi_{j\downarrow}$, and the orbitals are chosen self-consistently. Within such an approximation the tunneling current is

$$I = I_0\sum_{n\sigma}|\phi_{n\,\sigma}(k)|^2\,\delta(E_{n\,\sigma}-\mathcal{E}_f), \qquad (11)$$

where, $I_0 = T^2\delta V/(2\pi)\sqrt{m^*/2\mathcal{E}_f}$, $k = \sqrt{2m^*\mathcal{E}_f} - Q$, and we have assumed that $Q = eBd_t/\hbar > 0$. The tunneling current therefore measures the momentum space density of the particles at the Fermi surface. If there are no particles at the Fermi surface, then no current flows.

The delta functions in (11) are broadened by finite lifetime and finite temperature. In particular if there are two different states i, j with energies $E_{i/j}$, and inverse lifetimes Γ, which satisfy $|E_{i/j} - \mathcal{E}_f| \ll \Gamma$ or $|E_{i/j} - \mathcal{E}_f| \ll k_BT$, then the current is proportional to the incoherent sum

$$I \propto |\phi_i(k)|^2 + |\phi_j(k)|^2. \qquad (12)$$

This feature will be important in high symmetry situations where there is a near degeneracy (see, for example, section V A).

In the remaining sections of this paper, we calculate $\phi_j(k)$.

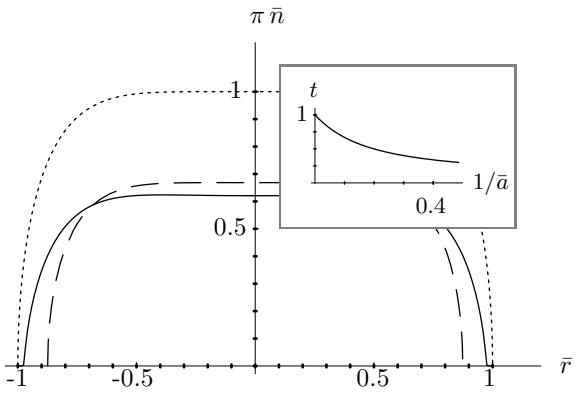

FIG. 2: Interaction induced change of dimensionless density $\bar{n}$ of spin-1/2 electron gas confined to a one-dimensional potential $V(x) \propto x^6$. Interaction parameters are $\bar{a} = 10$ and $\bar{d} = 10^{-3}$. Solid line: Equation (15) using regularization $f^{(2)}$; dashed line: approximation described above eq. (16); dotted line: noninteracting profile. Inset: Renormalized dimensionless cloud radius t as a function of $1/\bar{a}$ from solving eq. (16).

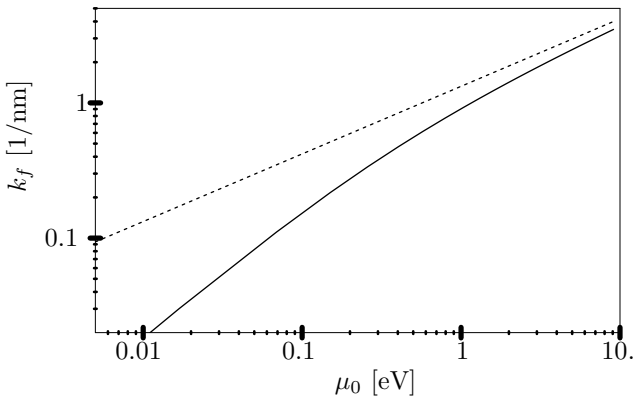

FIG. 3: Peak wavevector $k_f = tk_0$ of wavefunction at fermi surface as a function of chemical potential $\mu_0 = \hbar^2 k_0^2/2m^*$ within the Thomas-Fermi approximation. Dotted line shows noninteracting result, $t = 1$. Solid line includes Coulomb interactions with $a = 10nm$, $d_\perp = 20nm$, in a power law trap with $\beta = 6$ and $w = 3\mu$m. This approximation will break down when $k_f \lesssim 1/a$.

III. HIGH DENSITY: THOMAS-FERMI

The simplest picture of a gas of electrons in a confined geometry comes from the Thomas-Fermi (local density) approximation, where the system is described by a local chemical potential $\mu(x) = \mu_0 - V_{\rm eff}(x)$. The global chemical potential is $\mu_0 = \hbar^2 k_0^2/2m^*$, and the effective potential $V_{\rm eff}(x)$ includes both the external field and the interactions between the particles. Within the Hartree approximation, which is valid at high densities $na \gg 1$, the effective potential is

$$V_{\rm eff}(x) = \int dx'\, U(x-x')n(x'). \qquad (13)$$

The chemical potential is then related to the density by the relationship for a homogeneous gas, $\mu(r) = 2\pi^2\hbar^2 n^2/\sigma^2 m^*$. Self-consistency requires that the density obeys a nonlinear integral equation,

$$\mu_0 = V_{\rm ext}(x) + \int dx' U(x-x')n(r') + \frac{2\pi^2\hbar^2}{\sigma^2 m^*} n^2(r). \quad (14)$$

This local density approximation only makes sense if the density changes slowly compared to the interparticle spacing $[(\partial_x n(x))/n(x)^2 \ll 1]$. We write (14) in dimensionless form by introducing $k_0^2 = 2m^*\mu_0/\hbar^2$, $R^\beta = k_0^2 w^{2+\beta}$, $\bar{r} = r/R$, $\bar{a} = k_0 a$, $\bar{n} = k_0 n$, $\bar{d} = d/R$,

$$\frac{4\pi^2}{\sigma^2}\bar{n}^2(r) = 1 - \bar{r}^\beta - \frac{2}{\bar{a}}\int_{-1}^{1} f_{\bar{d}}(\bar{r}-\bar{r}')n(\bar{r}')d\bar{r}'. \qquad (15)$$

At fixed chemical potential the interactions can only reduce the density. Therefore the density is always bounded by the noninteracting result, $\bar{n}_0 = (\sigma/2\pi)\sqrt{1-\bar{r}^\beta}$. In particular, the density always vanishes for $\bar{r} > 1$. For very steep potentials, $\beta \to \infty$, the noninteracting Thomas-Fermi radius R approaches the trap length, $R/w \approx 1 + 2\beta^{-1}\log(k_0 w) + \mathcal{O}(\beta^{-2})$.

For $a \gg 1$, equation (15) can be solved iteratively[12]. In this limit, the interactions predominately renormalize the chemical potential. Approximating the integral in (15) by its value at $\bar{r} = 0$, one self-consistently finds that $(2\pi/\sigma)\bar{n}(\bar{r}) \approx \sqrt{t^2 - \bar{r}^\beta}$ where t solves the transcendental equation

$$t^2 = 1 - \frac{\sigma}{\pi\bar{a}} t(A + 4\log t). \qquad (16)$$

The parameter A depends logarithmically on the cutoff $d_\perp$. For the regularization f_2, $A = 1 - 4/\beta + (2/\beta)\log(4/d_\perp^\beta)$. Figure 2 compares this approximation to the numerical solution of (15), and the inset shows t as a function of $\bar{a}$.

A. Wavefunction of last occupied state

As previously explained, within an independent particle picture the tunneling current between two parallel wires is proportional to the momentum space wavefunction of the highest occupied single particle state. This momentum space wavefunction will be strongly peaked about $k_f(r = 0)$, which can be approximated as $k_0 t$, where $\hbar^2 k_0^2/2m^* = \mu_0$, and t is given by eq. (16). Figure 2 shows $k_f \equiv k_f(r = 0)$ as a function of μ_0 for reasonable parameters.

To go beyond this single wavevector approximation, we use semiclassical means to calculate the wavefunction of the state at the Fermi surface. We find the modulus by imagining that we reduce the chemical potential by a very small amount, so that this last state goes from filled to empty. The density change must coincide with the

density $n_f(r)$ of that last single particle state, implying that

$$n_f(x) = |\psi_f(x)|^2 = \Omega \frac{\partial n(r)}{\partial \mu_0}, \tag{17}$$

where Ω is a normalization constant determined by setting $\int n_f(x)\,dx = 1$. This wavefunction should have a phase whose derivative gives the local fermi momentum.

$$\frac{\partial \varphi_f(x)}{\partial x} = \pm\sqrt{2m^*\mu(x)} \equiv k_f(x). \tag{18}$$

The + and − solutions correspond to left-moving and right moving waves. In principle, one must combine these two solutions to form a standing wave. Within the Hartree approximation, this procedure is equivalent to finding the WKB wavefunction in the self-consistent potential. We do not discuss the details as when we compute the momentum space wavefunction, only the structure near $k = 0$ will be affected by how we superimpose these two solutions.

In the case where the Coulomb interaction can be neglected, equation (17) reduces to $|\psi_f(x)| \propto k_f(x)^{-1/2} \propto 1/\sqrt{\mu_0 - V_{\rm ext}(x)}$, and equation (18) becomes $\partial\varphi/\partial x = k_f(x)$. Not surprisingly, in this limit $\psi_f(x)$ is *exactly* the WKB wavefunction for an electron with energy μ_0 in the potential $V_{\rm ext}(x)$. Our arguments therefore reduce to the semiclassical arguments of Tserkovnyak et al.[6] for the noninteracting gas. The analysis is very similar for our approximation where $\bar{n}^2 \propto t^2 - \bar{r}^\beta$. Since interactions only renormalize the chemical potential, the derivative $\partial n^2(r)/\partial\mu_0$ is a constant, independent of space, and we can use the noninteracting result with a renormalized chemical potential. That is, we take $k_f(x) = \sqrt{t^2\mu_0 - V_{\rm ext}(x)} = k_0\sqrt{t^2 - \bar{x}^\beta}$.

Following Tserkovnyak et al.[6], we calculate the momentum space wavefunction, $\phi_f(q) = \int dx\,\psi_f(x)e^{-iqx}$ by Laplace's method. The Fourier integral is dominated by regions of space near where $q = \pm k_f(x)$. Moreover, since $\phi_f(q)$ is peaked around $q = \pm k_f(0)$, we can expand $\varphi(x)$ near $x = 0$. Since $|\phi_f(q)|$ is symmetric, there is no loss of generality in taking $q > 0$. We introduce $p = (k_f(0) - q)X$, with $X^{\beta+1} = 2k_f w^{\beta+2}$. Changing variables to $y = px/X$, and assuming $(k_f(0) - q) \ll k_f(0)$, we find

$$\frac{\phi_f(q)}{\Omega'} = \mathrm{Re}\left[\int_0^\infty dy \exp\left(ipy - i\frac{y^{\beta+1}}{\beta+1}\right)\right], \tag{19}$$

where Ω' is a normalization constant. In the case $\beta = 2$, the integral in (19) is an Airy function, though for other values of β it is not a familiar special function. The argument of the exponential, χ, is stationary at $y = y_0 = p^{1/\beta}$. The curvature is $\chi''(y_0) = -i\beta p^{1-1/\beta}$. This is an isolated saddle point when $y_0^2|\chi''(y_0)| = \beta|p|^{1+1/\beta} \gg 1$, in which case

$$\frac{\phi_f(q)}{\Omega'} = \mathrm{Re}\left[\sqrt{\frac{2\pi}{i\beta p^{1-1/\beta}}}\exp\left[i\frac{\beta p^{1+1/\beta}}{1+\beta}\right]\right]. \tag{20}$$

By deforming the contour of integration, this equation holds for both $p > 0$ and $p < 0$ (in the latter case one should take the principle branch, giving p a small negative imaginary part). From (20), one sees that if $\beta \neq \infty$, the wave function falls off exponentially as $p \to -\infty$. For $p \ll \beta^{\beta/(1+\beta)}$, instead of expanding about the saddle point, we expand about $y = 0$, finding as $p \to 0$,

$$\begin{aligned}\frac{\phi_f(q)}{\Omega'} &= \mathrm{Re}\left[(\beta+1)^{-\beta/(\beta+1)}\Gamma\left(\frac{1}{\beta+1}\right)e^{\Theta}\right] \\ \Theta &= p\,(\beta+1)^{1/(\beta+1)}\frac{\Gamma\left(\frac{2}{\beta+1}\right)}{\Gamma\left(\frac{1}{\beta+1}\right)}i^{1/(\beta+1)} \\ &\quad -i(\pi/2)(1/(\beta+1)).\end{aligned} \tag{21}$$

IV. LOW DENSITY: WIGNER CRYSTAL

In section III, we neglected the fact that electrons are discrete entities and that an electron does not interact with itself. Including this discreteness, the interaction energy can be reduced by localizing each electron to a small volume – maximizing the distance between the charge distribution of neighboring particles. Since such localization costs kinetic energy, it is only favorable in the low density gas where interaction energy dominates over kinetic energy.

To discuss this phase, we imagine that we have N electrons, localized at positions x_j where $j = 1, 2, \ldots, N$. Neglecting kinetic terms, the energy of a given configuration is

$$E = \sum_j V_{\rm ext}(x_j) + (1/2)\sum_{i\neq j} U(x_i - x_j). \tag{22}$$

As with the profile in the dense limit (fig. 2), we numerically find that the resulting density is quite flat, and is well approximated by evenly spaced electrons, $x_j n \approx j - (N+1)/2$, with uniform density n. Minimizing (22) with respect to n yields

$$\begin{aligned} n^{-1} &= \frac{2w}{N}\left[\frac{\beta+1}{2\beta}\frac{w}{a}N^2\left(\log N - \frac{1}{2}\right)\right]^{1/(\beta+1)} \\ &\approx \frac{2w}{N}\left[1 + \frac{1}{\beta+1}\log\left(\frac{wN^2\log N}{2a}\right) + \mathcal{O}(\beta^{-2})\right] \end{aligned} \tag{23}$$

In this Wigner crystal state, each electron is confined to a length $\ell < n^{-1}$. To calculate this length, and the wavefunction of the localized electron, we expand the potential in eq. (22) for small fluctuations in the position of one of the particles,

$$\frac{\partial^2 V}{\partial x_j^2} = V''_{\rm ext}(x_j) + \frac{2\hbar^2}{m^* a}\sum_{i\neq j}|x_i - x_j|^{-3}. \tag{24}$$

We approximate the sum over a finite number of particles by that of an infinite chain, taking $\sum_{i\neq j}|x_i - x_j|^{-3} \approx$

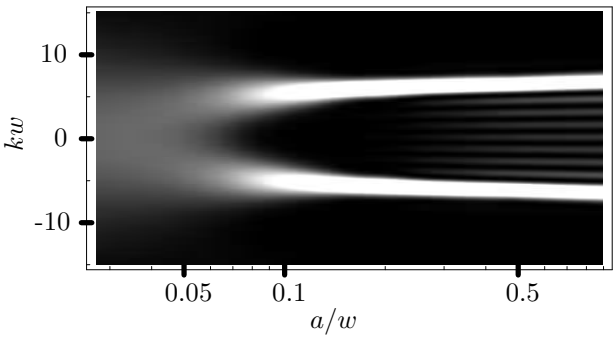

FIG. 4: Interaction dependence of the momentum space wavefunction of last single-particle state within the Hartree-Fock approximation. Eighteen particles are confined to the wire. Lighter colors correspond to larger values of $|\phi(k)|^2$. The horizontal axis shows different interaction strengths parameterized by the ratio of the Bohr radius a to the wire length w (note the logarithmic scale). The potential has exponent $\beta = 6$, and a cutoff, $d = 0.07w$.

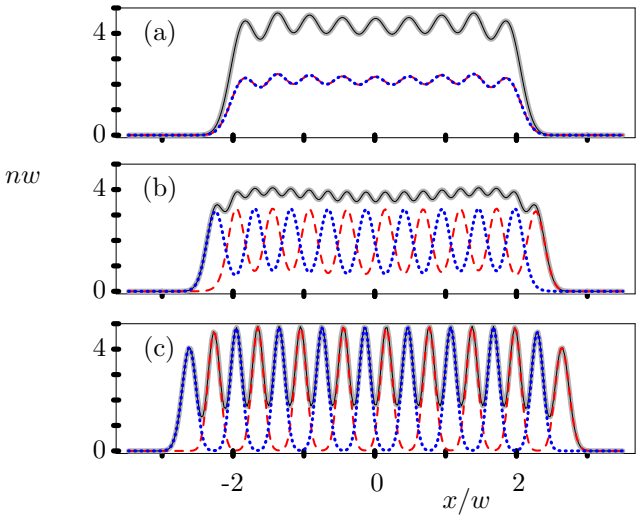

FIG. 5: (Color Online) Real space electron density n. Parameters coincide with Fig. 4. Solid, blue dotted, and red dashed lines correspond to total density and the density of up and down spin electrons [In (a), the latter two curves coincide]. Panels (a), (b), (c) correspond to a/w=0.5, 0.15, 0.05.

$2n^3 \sum_{l=1}^{\infty} l^{-3} = 2\zeta(3)n^3$. Numerically, the Riemann zeta function is $\zeta(3) \approx 1.2$. The curvature of the external potential is generically negligible in this limit, hence each electron is trapped by a harmonic oscillator potential with $m^*\omega_{\rm wc}^2 = (\hbar^2/m^*a)4\zeta(3)n^3$ and has a wavefunction $\psi_j(x) \propto \exp(-(x-x_j)^2/2\ell^2)$ with $\ell^4 = (\hbar/m^*\omega_{\rm wc})^2 = an^{-3}/(4\zeta(3))$. This implies that the momentum space wavefunction has modulus $|\psi_j(k)|^2 \propto \exp(-k^2\ell^2)$.

Comparing this momentum space wavefunction to the high density predictions [equation (19) through (21)], we see that in the Wigner crystal, $|\phi(q)|^2$ is more spread out in momentum space, and does not contain any oscillations.

V. HARTREE-FOCK STUDY OF CROSSOVER

We investigate the crossover between the high density electron gas and the low density Wigner crystal within the Hartree-Fock approximation. In the extreme limits, Hartree-Fock reduces to our previous approximations. It also provides semi-quantitative understanding of the intermediate regime. In uniform higher dimensional systems, Hartree-Fock overestimates the stability of the Wigner crystal[13], and one therefore expects some systematic errors as compared to an exact many-body calculation. This approximation also fails to capture more exotic effects of electron correlations, such as spin-charge separation. Experimental signatures of such effects are subtle[2], and as a first approximation it is quite reasonable to neglect them.

Hartree-Fock is most simply thought of as a variational method, where one searches for the Slater determinant which minimizes the energy[14]. This procedure is highly nontrivial as the energy landscape in the space of Slater determinants is quite complex with many local minima. We start by considering the limit of vanishing interactions ($a/w \to \infty$), where we find the exact solution by discretizing space and solving the single-particle Schrodinger equation. With fixed numbers of up and down spin electrons ($n_\uparrow$ and $n_\downarrow$), we then gradually decrease w/a. For each value of w/a we iteratively solve the Hartree-Fock equations in discretized space. Although there is no guarantee that the states we find in this manner are absolute energy minima, they consistently have lower energies than all other states that we have found by iterating the Hartree-Fock equations from different starting points.

An advantage of the Hartree-Fock approximation is that since it involves an independent electron approximation, one has direct access to single-particle observables, such as the wavefunction of the last bound state. Figure 4 shows the momentum-space wavefunction of the last bound state for a system of eighteen particles (nine in each spin state). For large a/w, this last single-particle state is delocalized in real space, resulting in a series of momentum-space peaks which are well described by equation (19). For small a/w, this last state is localized, resulting in a broad spread of momenta. Illustrative real-space density profiles are shown in figures 5 a,b,c. In (a) we see that even for arbitrarily weak interactions the real space density is corrugated. The corrugations are caused by the free electron response to an inhomogeneous potential and are analogous to the Friedel[15] oscillations seen in electron density near an impurity. The asymptotic behavior of these oscillations has been analytically calculated for harmonic confinement[16]. There are nine peaks corresponding to the nine doubly occupied single particle states. In (b) we see that as we increase the interaction strength each of the density peaks split into two, so there

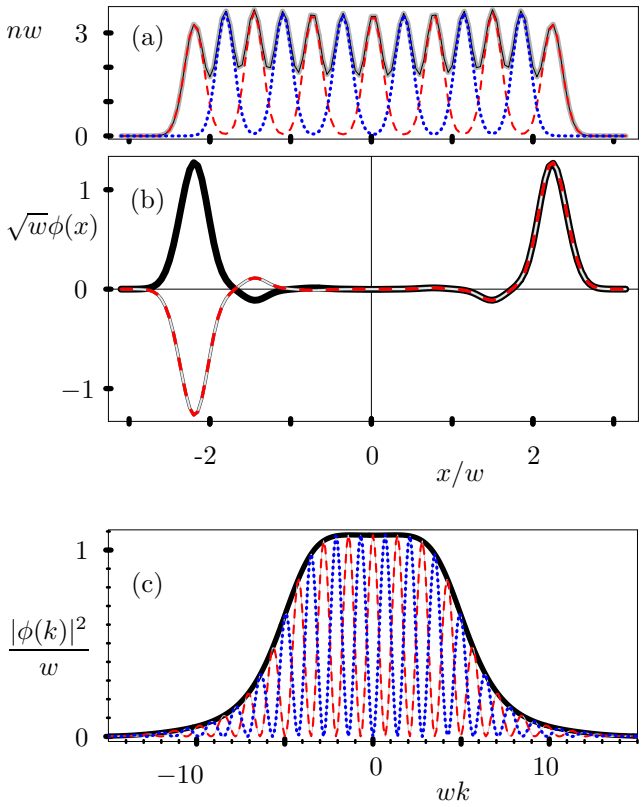

FIG. 6: (Color Online) (a) Density of 13 electrons with $a/w = 0.1$, see caption of fig 5 for key. (b) Wavefunction $\phi_i(x)$ (solid) and $\phi_j(x)$ (dashed) of the two highest highest energy occupied states. (c) Momentum space wavefunctions: red dashed, $|\phi_i(k)|^2$; blue dotted, $|\phi_j(k)|^2$; solid, $(|\phi_i(k)|^2 + |\phi_j(k)|^2)$.

is one peak per particle. A spin-density wave appears. In (c) we see a Wigner crystal with an antiferromagnetic spin profile. The density varies smoothly as one increases the interactions.

A. Fringes

When an odd number of particles form a Wigner crystal the highest occupied single particle state, with wavefunction $\phi_i(r)$, is in a symmetric superposition of two locations, as illustrated in figure 6, and has fringes in its momentum space wavefunction, $\phi_i(k)$. The next highest energy state, $\phi_j(r)$, is in the antisymmetric superposition of these same two locations, and has momentum space fringes which are 90 degrees out of phase with those for $\phi_i(k)$. Since the splitting between these two states is exponentially small, the tunneling current is proportional to $|\phi_i(k)|^2 + |\phi_j(k)|^2$ (see section II C), which, as illustrated in figure 6c, contains no fringes.

VI. RELATED SYSTEMS

The crystallization described here is also highly relevant for studies of carbon nanotubes. Recent experiments on conducting tubes with extremely small electron densities show behavior which can be interpreted in terms of Coulomb induced localization of the electrons[17]. These systems are slightly more complex than the one discussed here because of the additional quantum numbers associated with the chirality of the electron motion as it follows a spiral path along the tube.

VII. SUMMARY

We have given simple analytic theories of very high and very low density electrons in an inhomogeneous one dimensional potential. Using the Hartree-Fock approximation we then numerically studied the cross-over between these limits. One expects that this approximation will overestimate the stability of the crystalline phase, while providing excellent qualitative understanding of the crossover.

Acknowledgments

I would like to thank Amir Yacoby for providing experimental details[3], Bertrand Halperin for stimulating correspondence, and Paul McEuen for discussing related experiments on carbon nanotubes. This work was partially performed at the Kavli Institute for Theoretical Physics. It was supported in part by the National Science Foundation under Grant No. PHY99-07949.

[1] A. Yacoby, H, K, Stormer, N. S. Wingreen, L. N. Pfeiffer, K. W. Baldwin, and K. W. West, Phys. Rev. Lett. **77**, 4612 (1996); Solid State Communications **101**, 77 (1997); L. N. Pfeiffer, A. Jacoby, H. L. Stormer, K. W. Baldwin, J. Hasen, A. Pinczuk, W. Wegscheider, and K. W. West, Microelectron. J. **28**, 817 (1997).

[2] O. M. Auslaender, A. Yacoby, R. de Picciotto, K. W. Baldwin, L. N. Pfeiffer, and K. W. West, Science **295**, 825 (2002).

[3] H. Steinberg, O. M. Auslaender, A. Yacoby, J. Qian, G. A. Fiete, Y. Tserkovnyak, B. I. Halperin, R. de Picciotto, K. W. Baldwin, L. N. Pfeiffer and K. W. West, *Localization Transition in Ballistic Quantum Wires*, unpublished (2004). Also see D. Yacoby, *Measurement of Spin Charge Separation and Localization in 1D*, Lecture at KITP, 5/20/2004. `http://online.kitp.ucsb.edu/online/exotic04/yacoby/`

[4] E. Wigner, Phys. Rev. **46**, 1002 (1934); Trans. Faraday Soc. **34**, 678 (1938).

[5] The Mermin-Wagner theorem [N. D. Mermin, and H. Wag-

ner, Phys. Rev. Lett. **17**, 1133 (1966)] prohibits long-range crystalline order in one dimension, but does not restrict the short-range order or localization described here.

[6] Y. Tserkovnyak, B. I. Halperin, O. M. Auslaender, and A. Yacoby, Phys. Rev. Lett. **89**, 136805 (2002); Y. Tserkovnyak, B. I. Halperin, O. M. Auslaender, and A. Yacoby, Phys. Rev. B **68**, 125312 (2003).

[7] B. Tanatar, I. Al-Hayek, and M. Tomak, Phys. Rev. B **58**, 9886 (1998). L. I. Glazman, I. M. Ruzin, and B. I. Shklovskii, Phys. Rev. B **45**, 8454 (1992). H. J. Schulz, Phys. Rev. Lett. **71**, 1864 (1993). Q. Yuan, H. Chen, Y. Zhang, and Y. Chen, Phys. Rev. B **58**, 1084 (1998). G. Fano, F. Ortolani, A. Parola, and L. Ziosi, Phys. Rev. B **60**, 15654 (1999).

[8] W. Häusler and B. Kramer, Phys. Rev. B **47**, 16353 (1992). B. Szafran, F. M. Peeters, S. Bednarek, T. Chwiej, and J. Adamowski, Phys. Rev. B **70**, 035401 (2004).

[9] E. Räsänen, H. Saarikoski, V. N. Stavrou, A. Harju, M. J. Puska, and R. M. Nieminen, Phys. Rev. B **67**, 235307 (2003). F. Anfuso, and S. Eggert, Phys. Rev. B **68**, 241301 (2003).

[10] As the chemical potential difference between the wires, δV depends not only on the applied potential, but also on the number of electrons in the short wire.

[11] Thus we neglect correlations between the two wires caused by the Coulomb interaction.

[12] For example, the first correction involves setting $\bar{n}(\bar{r}') = \bar{n}_0(\bar{r}')$ on the right hand side of (15). Using regularization f_2 this correction is $(4\pi^2/\sigma^2)(\bar{n}^2(\bar{r}) - x\bar{n}_0) \approx -(\sigma/\pi a)(A + B\bar{r}^2 + \mathcal{O}(\bar{r}^4))$, where $A = 1 - 4/\beta + (2/\beta)\log(4/d_\perp^\beta)$, and $B = [n\sqrt{\pi}\Gamma(1-2/\beta)]/[(n-4)\Gamma(1/2-2/\beta)]$.

[13] See J. R. Trail, M. D. Towler, and R. J. Needs, Phys. Rev. B **68**, 045107 (2003), and references therein.

[14] N. W. Ashcroft and N. D. Mermin, Solid State Physics (Hartcourt Brace, Fort Worth 1976).

[15] J. Friedel, Nuovo Cimento Suppl. **7**, 287 (1958).

[16] E. J. Mueller, cond-mat/0405425 *to appear in Phys. Rev. Lett.*.

[17] Pablo Jarillo-Herrero, Sami Sapmaz, Cees Dekker, Leo P. Kouwenhoven, and Herre S.J. van der Zant, Nature **429**, 389 (2004).